

A Statistical Description of the Microstructure of Young Sea Ice

DONALD K. PEROVICH AND ANTHONY J. GOW

U.S. Army Cold Regions Research and Engineering Laboratory, Hanover, New Hampshire

In order to fully exploit microwave models of sea ice, the standard ice characterization must be supplemented by a statistical description of the ice microstructure. For the strong fluctuation theory this statistical description takes the form of the mean and variance of the permittivity plus correlation lengths. We have computed these statistics for over 50 samples of young ice, including both columnar congelation ice and desalinated bubbly ice. Samples were taken from different vertical depths and horizontal positions within the ice sheet and encompassed a comprehensive range of ice temperatures and brine volumes. For each of these samples, horizontal thin sections were photographed, then digitized and analyzed on a personal computer-based image processing system. Results indicate that correlation lengths correspond to the physical dimensions of the inclusions: the brine pocket size (typically tenths of a millimeter) for saline ice and the air bubble size (typically millimeters) for desalinated ice. For saline ice the shape of the correlation function was elliptical, similar to the shape of the brine pockets. In one case as the ice warmed from -20° to -1°C and the brine volume increased from 2 to 37‰, the correlation length increased from 0.14 to 0.22 mm.

INTRODUCTION

Over the past several years there has been an increased interest in using microwave remote sensing observations to monitor geophysical processes in sea ice. During this period there has also been a growing awareness that in order to interpret these observations, an understanding of how variations in microwave signatures relate to differences in the physical properties and crystalline structure of the ice cover is necessary. Because of this, ice characterization has become an integral part of sea ice microwave remote sensing experiments [Arcone *et al.*, 1986; Tucker *et al.*, 1987]. This characterization typically has consisted of a description of ice surface conditions and vertical profiles of ice crystal structure, temperature, salinity, brine volume and density. Such characterizations have been shown to play a vital role in interpreting both passive and active microwave data [Tucker *et al.*, 1991].

However, for all their utility, such descriptive characterizations are not sufficiently detailed for microwave theoretical models. Winebrenner *et al.* [1989] have discussed the importance of a statistical description of ice structure and have enumerated several sea ice statistical measures needed for the evaluation of various microwave models. In this paper we shall explore a statistical description of sea ice suited for one prominent volume-scattering microwave model, the strong fluctuation theory. In this theory the medium is treated as though its permittivity is a random function of position [Tsang and Kong, 1981; Stogryn, 1984] and it is the distribution and the strength of the permittivity fluctuations that must be specified [Vallese and Kong, 1981; Lin *et al.*, 1988]. J. A. Kong (personal communication, 1988) has defined the elements needed to provide the statistical description of sea ice necessary for random media models: (1) the mean permittivity, (2) variance of the permittivity, (3) tilt of the optic axis of the permittivity tensor, and (4) correlation lengths in the X - Y , X - Z and Y - Z planes. The importance and the application of such a description to

microwave random media models of sea ice are discussed in detail by Tsang *et al.* [1985] and Lin *et al.* [1988].

Vallese and Kong [1981] examined correlation functions for snow and lake ice and found the functions to be exponential with correlation lengths corresponding to the average grain size for snow and the average bubble size for lake ice. Correlation functions for sea ice were investigated by Lin *et al.* [1988] in a combined experimental and theoretical effort. They analyzed a single horizontal thin section photograph and found that the correlation function was exponential. Indications were that the correlation lengths were comparable to the average size of the brine inclusions.

In this paper we will present results from an experimental program using laboratory-grown saline ice to investigate correlation functions for young sea ice. The focus is on determining correlation functions for sea ice and relating them to the physical properties and crystalline structure of the ice. Results are presented for different ice types including columnar congelation ice and desalinated columnar-textured bubbly ice. In addition, the influence of such parameters as growth rate, salinity and brine volume on the correlation function is discussed.

MEASUREMENT TECHNIQUES

During the past several years a program designed to evaluate the relationship of remote sensing signatures to the salinity and structural characteristics of saline ice has been conducted at the Cold Regions Research and Engineering Laboratory (CRREL). Saline ice sheets from which samples were periodically harvested for the present study were grown in an outdoor pond filled with water of salinity 24‰. Active and passive microwave measurements and a characterization of the ice structure were made of this ice.

Ice growth in the pond was initiated by spray seeding the surface of water with a high-pressure nozzle. This technique nucleates growth of congelation crystals with textures closely simulating those observed in Arctic sea ice. Such ice typically consists of vertically elongated columnar crystals composed of vertical plates of pure ice separated by parallel layers of brine inclusions. This sandwichlike substructure of the ice crystals reflects the process by which excess brine at

the growing ice/water interface is systematically incorporated between the individual plates of a crystal. Virtually no brine or salt is incorporated in the ice itself. Subsequent changes in the saline ice substructure occur mainly in response to temperature changes in the ice. Brine inclusions are especially responsive in this regard. In the event of prolonged warming of the ice, brine inclusions tend to coalesce and channelize, a situation leading ultimately to brine drainage and major changes in the geometry of the inclusions and concentration of entrapped brine. Such a process is exemplified in nature by the transformation of first-year ice to second-year and multiyear ice.

Once freezing of a saline ice sheet had begun it was closely monitored for salinity and structure changes during the course of its growth. Samples were obtained by sawing slabs from the ice sheet and storing them in a -25°C cold room for safekeeping prior to analysis. Salinities of melted samples were measured with a Beckman Solubridge, which had an estimated measurement precision of 0.2%. Studies of ice microstructure were made via thin sections prepared on a microtome at -10°C . For the purposes of this study the sections were photographed in plain light in order to highlight brine inclusion characteristics. The photographs were made at a 7X magnification using a 125 by 175 mm bellows extension camera. These observations are best made in horizontal thin sections which, by virtue of the vertical interdendrite nature of brine incorporation, provide a more thorough picture of brine pocket structure than vertical sections. Because of this, vertical thin sections of saline ice were not examined.

Once a suitable thin section photograph was obtained it was analyzed on a personal computer using the image processing software discussed by *Perovich and Hirai* [1988]. First a frame-grabber digitizes the thin section photograph into a 640×480 array of pixels with each pixel assigned a gray shade ranging from 0 (black) to 255 (white). The next stage is to partition the image into its constituent components. While sea ice is a four-component system consisting of ice, brine, air and solid salts, we shall approximate it by a two-component system of either ice and brine or ice and air. Solid salts were ignored since they did not constitute a significant portion of any of our samples. Though ice, brine and air may all have been present, it is very difficult, if not impossible to accurately distinguish between an air inclusion and a brine pocket using visual techniques. This forces us to make a simplifying assumption. In freshly grown saline ice the volume of brine greatly exceeds that of air trapped in the ice. Hence we assumed that the air volume is negligibly small and that all inclusions were brine filled. However, in bubbly desalinated ice, salinities can be so reduced by drainage that most of the inclusions can be assumed to be vapor filled.

The partitioning between the two components is done by exploiting the differences in gray shade between ice and its inclusions. Therefore it is critical that the thickness of the thin sections be constant and the illumination of the photographs be uniform. The brine volume of a sample was independently determined by inputting measured values of ice temperature and salinity into the relationship of *Frankenstein and Gardner* [1967]

$$v_b = S(0.0532 - 4.919/T), \quad -22.9 < T < -0.5^{\circ}\text{C}$$

where v_b is the percent brine volume, S is the salinity in per mil, and T is the temperature in degrees Celsius.

Each pixel was then assigned an integer gray shade appropriate to its permittivity, transforming the thin section photograph into an image of the spatial distribution of the permittivity. A value of 1 was used for air, 3 for ice and 80 for brine [*Vant et al.*, 1978]. A 400×400 main image and a 200×200 subimage were selected and the correlation function of the subimage with the main image was computed. The correlation function is defined as

$$R(x, y) = \frac{1}{\sigma_F \sigma_G} \sum_{j=1}^N \sum_{i=1}^M F(i, j) G(x+i, y+j) - \mu_F \mu_G$$

where μ_F , μ_G and σ_F , σ_G are respectively the mean and standard deviation of the subimage F and the main image G [*Papoulis*, 1965; *Lin et al.*, 1988] and m and n are the number of points in X and Y . $R(x, y)$ can range from -1 to 1 , with a value of 1 indicating perfect agreement between image and subimage, 0 meaning no relationship and -1 resulting from a comparison of a subimage with its complement. Correlation lengths are extracted from the correlation function by measuring the e -folding distance. The mean (μ) and variance (σ^2) of the image and subimage are calculated using the following expressions:

$$\mu = \frac{1}{mn} \sum_{j=1}^N \sum_{i=1}^M G(i, j)$$

$$\sigma^2 = \frac{1}{mn} \sum_{j=1}^N \sum_{i=1}^M [G(i, j) - \mu_G]^2$$

For a two-component system the mean and variance can also be computed from the fractional volume of the inclusion (f) using

$$\mu = f e_f + (1-f) e_i$$

$$\sigma_G^2 = f(e_f - \mu)^2 + (1-f)(e_i - \mu)^2$$

where e_i and e_f are the permittivities of ice and the inclusion. For a two-phase mixture it is straightforward to extend the results to any other frequency merely by changing the permittivity in the above equations to the value appropriate for that frequency. The correlation length does not depend on the value of the permittivity and thus is independent of frequency.

RESULTS

Over 50 correlation functions were calculated using horizontal thin sections from the 1988 and 1989 CRREL pond experiments. Most of the cases examined were young columnar ice, though an example of desalinated ice is also included. Samples were selected to include a range of temperatures, salinities and brine volumes. Spatial variability was also examined by taking thin sections from different depths and different horizontal positions in the ice cover. In this section we (1) present a representative sample case of columnar ice, (2) investigate the influence of changes in temperature and brine volume, (3) examine how the corre-

lation function is affected by vertical and horizontal variability of the ice, and (4) present results from desalinated ice.

Sample Case: Columnar Ice

Most of the ice studied during the CRREL pond experiments was obtained from sheets seeded prior to freezing. Because of this, columnar ice was the predominant ice type observed. Figure 1a is a photograph of a horizontal thin section taken from the bottom of a 95-mm-thick ice sheet that had been growing for 48 hours. The ice was columnar with the c axes of the component crystals being substantially horizontal. The salinity of the sample was 11‰ and the ice temperature was -10°C when the photograph was taken, giving a brine volume of 6.1%. The digitized version of this photograph is shown in Figure 1b. Knowing the brine volume we divided the digitized image into its constituent components of ice (white) and brine (black) (Figure 1c). The 400×400 main image and 200×200 subimage were then selected as defined by the long and short pairs of vertical lines in Figure 1c. The subimage was overlain at every other point of the main image and the correlation function was computed. The two-dimensional correlation function $R(x, y)$ calculated for this image is plotted in Figure 1d. It is peaked with a sharp dropoff and small, regular sidelobes. Expanding the scale (Figure 1e), $R(x, y)$ is seen to be more elliptical than circular, with correlation lengths in the major and minor directions of 0.15 and 0.09 mm. Looking at the brine inclusions in Figure 1c we find that they have a mean cross-sectional area of the order of 0.028 mm^2 . Thus, as was the case for *Lin et al.* [1988], the correlation function is closely associated with the physical size of the brine inclusions. The mean and variance of the permittivity for this thin section are 9.6 and 467.

Effects of Temperature

The microstructure of sea ice is strongly affected by temperature. For example, as cold ice below the eutectic temperature warms, the crystallized salts come into solution. As warming continues the brine volume increases, changing the size and spatial distribution of the brine inclusions. This, in turn, will have an effect on the correlation function. To investigate this we performed a simulated warming of a thin section photograph.

The sample was columnar with horizontal c axis and had a salinity of 6.8‰ and was taken from a depth of 0.22 m in an ice cover that was 0.23 m thick. Figure 2a shows a photograph of the sample taken at -10°C . In addition to the standard image analysis, the brine volume was calculated for temperatures of -20° , -5° , -2.5° and -1°C , and the gray shade range assigned to brine was adjusted to simulate the change in brine volume with temperature. This computer simulation agreed well with qualitative observations of changes in the brine distribution during ice warming [*Perov-*

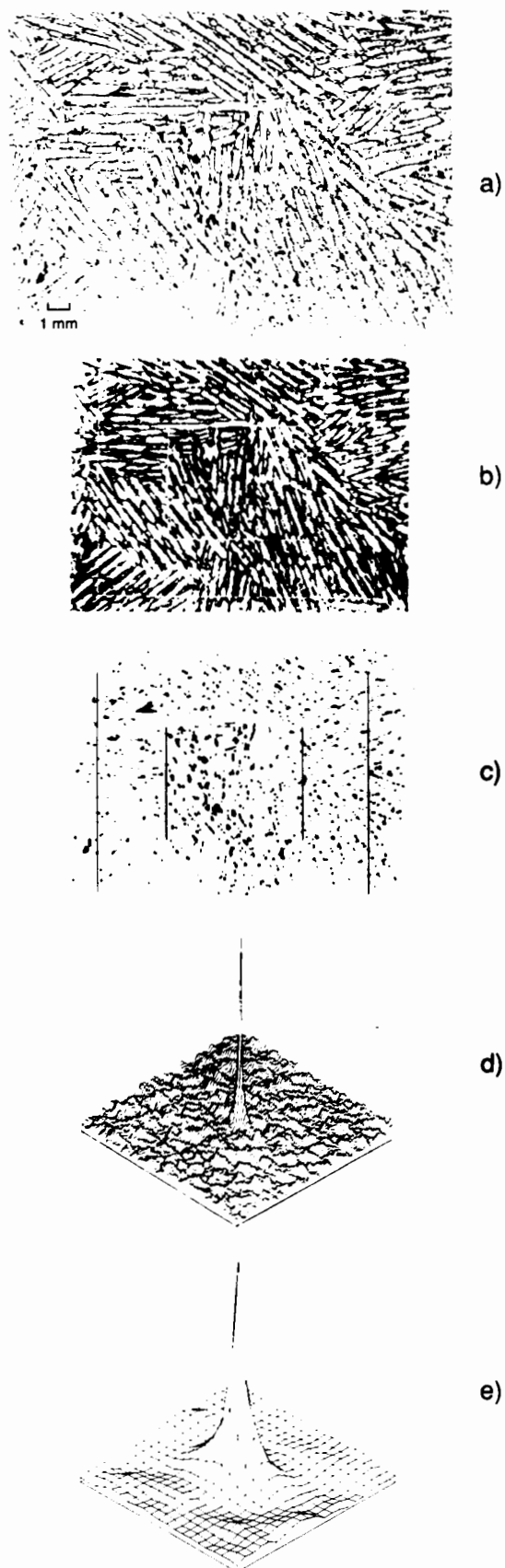


Fig. 1. (Opposite) Sample case of young saline ice which had been growing for 48 hours: (a) horizontal thin section taken from the bottom of 95-mm-thick ice, (b) digitized version of the photograph, (c) digitized image divided into its constituent components of ice (white) and brine (black) with the image and subimage denoted by the long and short pairs of vertical lines, (d) the full correlation function, and (e) an enlargement of the peak of the correlation function. The brine volume was 6.1%. The horizontal scale is 1 mm.

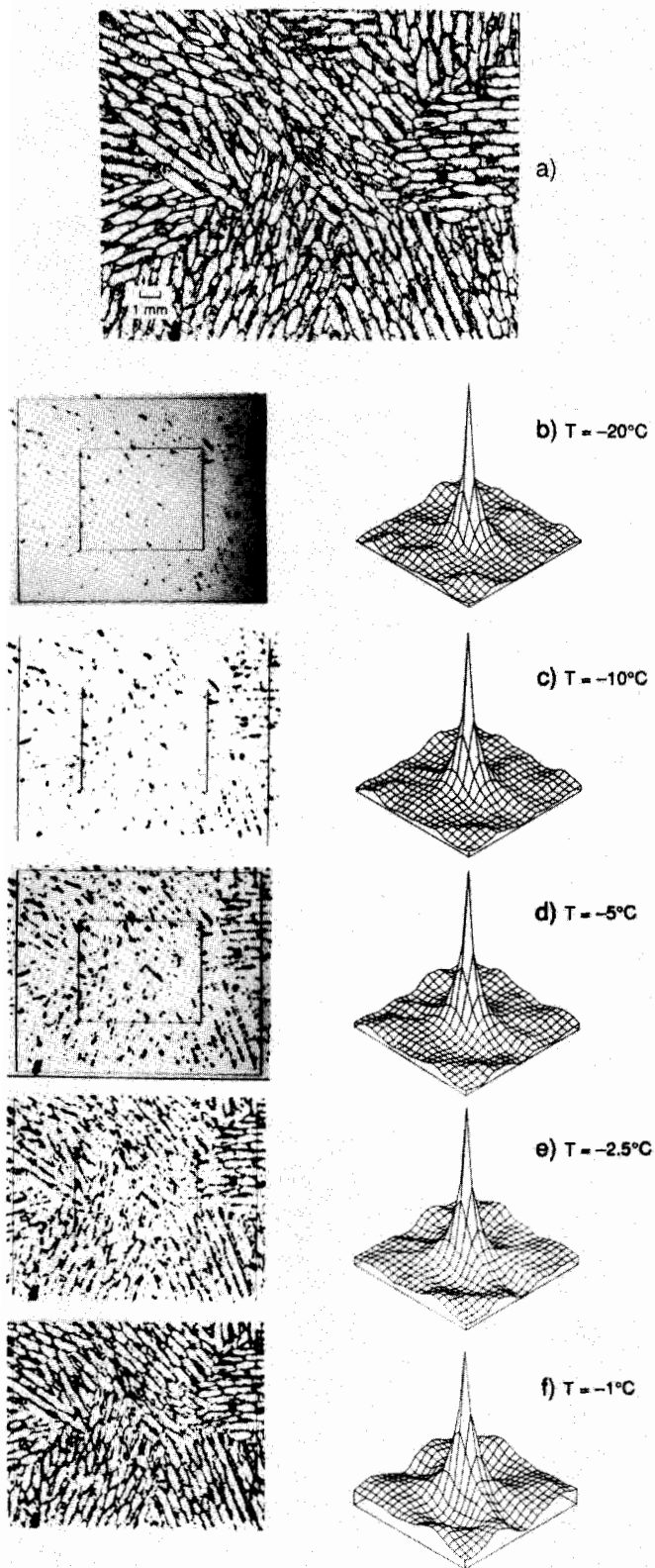


Fig. 2. The effects of ice temperature, and therefore brine volume, on the correlation function. (a) A horizontal thin section from near the bottom of a 0.23-m-thick ice sheet. The section had a salinity of 6.8‰. (b)–(f) Digitized image partitioned into ice (white) and brine (black) and the associated correlation functions for (b) $T = -20^{\circ}\text{C}$, $v_b = 1.9\%$, (c) $T = -10^{\circ}\text{C}$, $v_b = 3.7\%$, (d) $T = -5^{\circ}\text{C}$, $v_b = 7.5$, (e) $T = -2.5^{\circ}\text{C}$, $v_b = 15\%$, and (f) $T = -1^{\circ}\text{C}$, $v_b = 37.4\%$.

ich and Grenfell, 1981; Arcone *et al.*, 1986]. One limitation of the simulation is that it does not consider brine drainage, which can be an important process as the brine volume increases. Figures 2b–2f illustrate changes in the brine distribution and in the correlation function during simulated warming from -20°C to -1°C . The relevant statistics for this simulation are summarized in Table 1. During this warming the brine volume increased from 1.9% to 37.4% resulting in an increase in the mean permittivity of the medium by nearly an order of magnitude from 4.2 to 33.3. As the brine volume increased there was a corresponding broadening of the correlation function along with an increase in the correlation lengths. This is not surprising in light of the relationship between the correlation function and the size of the brine inclusions; as the ice warms, the size of the brine inclusions increases, and the correlation lengths increase.

In addition to the broadening of the peak there is also an increase in the amplitude of the sidelobes on the correlation function. This is illustrated in Figure 2f where the brine pockets have become so numerous as to essentially outline the ice platelets and there is a marked increase in the amplitude of sidelobes in the correlation function. The spacing of these secondary peaks is of the same order as the size of the ice platelets. Thus for large brine volume, the main contribution to the correlation function is still due to the size of the brine inclusion, but there is an additional, though lesser, contribution due to the width of the ice platelets.

Vertical Variability

Sea ice properties typically exhibit a great deal of vertical variability. To see if this variability extends to the correlation function we shall examine results from 120-mm-thick young ice. Figure 3 shows vertical profiles of salinity, temperature, brine volume and ice structure for this ice sheet. The temperature profile is linear with cold temperatures at the surface and warm temperatures at the ice-water interface. The salinity profile exhibits a characteristic *c* shape with values ranging from 5.4 to 6.4‰. Brine volume is fairly constant at 3% down to a depth of 60 mm, then it increases at an increasing rate reaching a value of 28% at the bottom of the ice sheet. Structurally, the ice consisted of a thin (2 mm) granular layer underlain by columnar ice. The *c* axes of the congelation ice crystals had become substantially horizontal by a depth of 70–80 mm.

We analyzed thin sections taken at depths of 30, 55, 90 and 120 mm from this ice sheet. Thin section photographs and the associated correlation functions are shown in Figure 4 with pertinent statistics summarized in Table 1. Texturally, the sections are very similar except for the bottom ice section which, as depicted here, consists essentially of just a single crystal with appreciably wider brine layer spacings than in the ice above. This broad spacing of the brine layers can probably be attributed to slower growth.

Vertical variability is also evident in the correlation functions. Based on the results from the temperature dependence simulation we would expect that, like the brine volume, the correlation lengths would increase with depth. While this is generally true, the actual depth dependence of the correlation function is more complicated. Indeed, in Figure 4 the correlation length was largest at the bottom, where the large brine volume resulted in a pronounced broadening of the

TABLE 1. Summary of Ice Statistical Parameters

| Figure | Depth, mm | Temperature, °C | Salinity, ‰ | Brine Volume, ‰ | Mean | Variation | <i>a</i> , mm | <i>b</i> , mm | <i>a/b</i> |
|----------------------------------|-----------|-----------------|-------------|-----------------|------|-----------|---------------|---------------|------------|
| <i>Sample Case: Columnar Ice</i> | | | | | | | | | |
| 1 | 95 | -10.0 | 11.0 | 6.1 | 9.6 | 465 | 0.15 | 0.12 | 1.3 |
| <i>Effects of Temperature</i> | | | | | | | | | |
| 2 <i>b</i> | 220 | -20.0 | 6.8 | 1.9 | 4.2 | 94 | 0.14 | 0.11 | 1.3 |
| 2 <i>c</i> | 220 | -10.0 | 6.8 | 3.7 | 5.9 | 213 | 0.16 | 0.14 | 1.1 |
| 2 <i>d</i> | 220 | -5.0 | 6.8 | 7.5 | 8.9 | 424 | 0.17 | 0.15 | 1.1 |
| 2 <i>e</i> | 220 | -2.5 | 6.8 | 15.0 | 14.5 | 751 | 0.18 | 0.15 | 1.2 |
| 2 <i>f</i> | 220 | -1.0 | 6.8 | 37.4 | 33.3 | 1414 | 0.22 | 0.16 | 1.4 |
| <i>Vertical Variability</i> | | | | | | | | | |
| 4 <i>a</i> | 30 | -11.9 | 6.4 | 3.0 | 5.7 | 204 | 0.22 | 0.19 | 1.2 |
| 4 <i>b</i> | 55 | -8.7 | 5.7 | 3.6 | 5.8 | 207 | 0.22 | 0.15 | 1.5 |
| 4 <i>c</i> | 90 | -4.3 | 5.4 | 6.9 | 8.2 | 376 | 0.13 | 0.11 | 1.2 |
| 4 <i>d</i> | 120 | -1.2 | 6.2 | 28.4 | 24.8 | 1203 | 0.32 | 0.17 | 1.9 |
| <i>Horizontal Variability</i> | | | | | | | | | |
| 5 <i>a</i> | 65 | -10.0 | 11.0 | 6.1 | 7.4 | 320 | 0.21 | 0.14 | 1.5 |
| 5 <i>b</i> | 65 | -10.0 | 11.0 | 6.1 | 7.9 | 353 | 0.13 | 0.13 | 1.0 |
| 5 <i>c</i> | 65 | -10.0 | 11.0 | 6.1 | 8.1 | 365 | 0.26 | 0.21 | 1.2 |
| <i>Desalinated Ice</i> | | | | | | | | | |
| 6 <i>a</i> | 3 | -10.0 | 0.0 | 0.0 | 2.8 | 0.4 | 2.00 | 2.00 | 1.0 |
| 6 <i>b</i> | 30 | -10.0 | 0.0 | 0.0 | 2.8 | 0.4 | 2.00 | 1.10 | 1.8 |

The mean and variance are reported for the permittivity of the main image, and *a* and *b* are the correlation lengths along the major and minor axis of the ellipse. All data are for horizontal thin sections, with the exception of Figure 6*b*.

correlation function peak. However, the smallest correlation lengths (0.13 mm, 0.11 mm) were at a depth of 90 mm, which had a brine volume larger than the 30- or 55-mm sections. This can be explained by examining the thin sections. The ice platelets were smaller at 90 mm, and the brine was distributed among many smaller inclusions. Thus the correlation function is not related simply to the volume of brine, but also to its distribution. Comparing Figures 4*c* and 4*d* we see a difference in orientation in the peak of the correlation function. We see that in both cases the peak is aligned with the direction of the platelets which govern the orientation of the brine pockets. These results indicate that there is sufficient vertical variation so that data from a single depth do not accurately represent the entire ice cover.

Horizontal Variability

Typically, horizontal variations in properties of young sea ice are small. For example, measurements of closely spaced samples of freshly grown columnar-textured saline ice showed minimal horizontal variability of salinity. However, with increasing thickness and aging of the ice, thermally induced redistribution of the entrapped brine can lead to differences in salinity over short horizontal distances. This situation has been established for thick Arctic first-year ice sampled at the end of winter [Untersteiner, 1968; Tucker *et al.*, 1984]; differences of up to 2‰ at corresponding depths have been reported by Tucker *et al.* [1984] who ascribed such variation to differential brine drainage due to the variable location of brine drainage channels.

To examine the question of horizontal variability of the correlation function we analyzed samples from three different locations a few meters apart in a uniformly grown ice cover. All three samples were taken near the bottom of a

65-mm-thick ice cover and all had the same salinity and brine volume. Thin section photographs for the three sites are shown in Figure 5.

At first glance the photographs show a similar columnar structure with *c* axis horizontal and elongated, orderly ice platelets of comparable size. While the photographs are visually similar, there are significant differences not only in the magnitude of the correlation function, but also in the shape. The correlation functions are elliptical for Figures 5*a* and 5*c* and circular for Figure 5*b*, with correlation lengths ranging from 0.13 to 0.26 mm. It is difficult to know precisely to what structural features of the ice to ascribe these differences. Looking more closely at the photographs we do see that the ice crystals are larger in Figure 5*a* and that in Figure 5*c* the brine inclusions are somewhat bigger. The important point is that differences in the correlation function, over small spatial scales, exist even in ice that is relatively homogeneous. We expect that even greater differences would exist in thicker aged first-year ice and in multiyear ice.

Desalinated Ice

The previous examples were obtained from saline, columnar, young ice at various stages of growth. In this section we shall briefly examine an additional ice type, desalinated ice. We simulated desalinated ice by removing a 0.16-m-thick saline ice sheet in large slabs from the sea ice pond, then allowing the ice to weather and desalinate for one month. Salinities of the desalinated ice were near zero with densities between 0.84 and 0.87 Mg/m³ and porosities between 5.5 and 8.5%. A crystallographic examination of the desalinated ice showed a substantial disappearance of ice platelet/brine layer substructure, and an overall retexturing of the crystals.

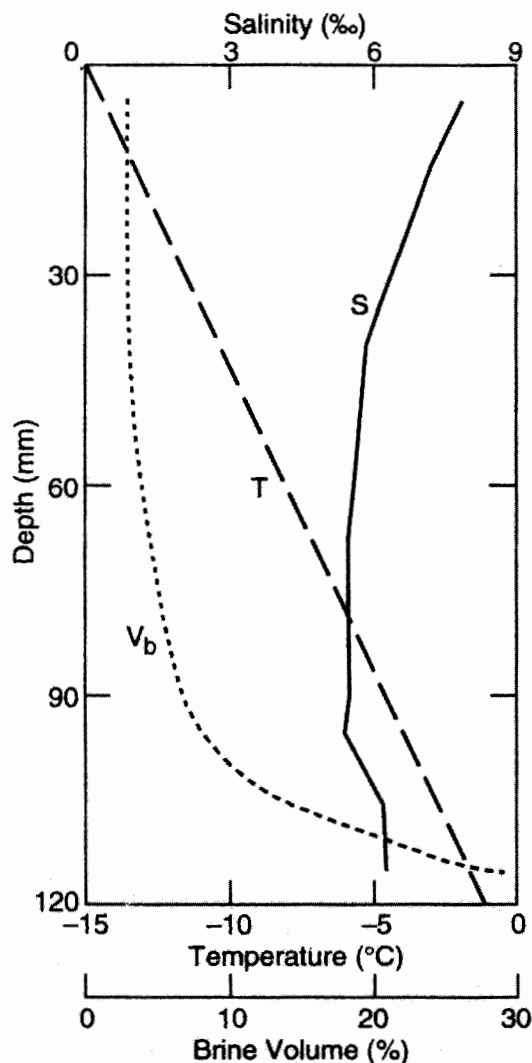


Fig. 3. Vertical profiles of temperature (T), salinity (S) and brine volume (v_b) for young, columnar, saline ice.

The texture of this ice was similar to the subsurface portion of the multiyear ice and to glacial ice.

As before, the digitized images were partitioned by exploiting differences in gray shade; for desalinated ice the two components were ice and air. A permittivity of 3 was assigned to the ice and 1 to the air. Figure 6 shows horizontal (Figure 6a) and vertical (Figure 6b) thick section photographs from the top portion of a desalinated ice cover. Note that the scale in this figure is larger than for the other figures. The appearance of this ice is clearly different from the saline ice discussed earlier, with the major structural features being the air bubbles, rather than the ice platelets and the brine inclusions. One benefit of this structural difference is that for the desalinated ice a meaningful analysis of vertical thin sections was possible.

The difference in structure is also manifested in the statistical properties of the ice as the correlation functions plotted in Figure 6 indicate. The horizontal section has a very broad and symmetric correlation peak. The correlation length is 2 mm, an order of magnitude larger than the saline ice cases. For desalinated ice the correlation length corresponds to the dimensions of the air bubbles, which are much larger than the brine inclusions in the saline ice. The corre-

lation function for the vertical section shows greater asymmetry with lengths of 2.0 and 1.1 in the major and minor directions. This is not surprising since the air bubbles are vertically oriented elongated ellipsoids. Thus the bubbles look circular in horizontal cross section and elliptical in vertical cross section. Lacking brine, both the mean (2.8) and the variance (0.4) of the permittivity are much smaller for desalinated ice.

CONCLUSIONS

Correlation lengths for sea ice are directly related to physical features of the ice microstructure, such as the size of brine pockets in young ice (typically tenths of a millimeter) and vapor inclusions in desalinated ice (typically millimeters). Like the ice microstructure, the correlation function of sea ice can be quite variable, depending on such parameters as growth conditions, ice temperature and brine volume. Warming causes brine inclusions to grow and correlation lengths to increase. Even a uniformly grown ice cover exhibits significant horizontal differences in brine inclusion characteristics and attendant variations in correlation length. In the vertical, a growing ice sheet has the

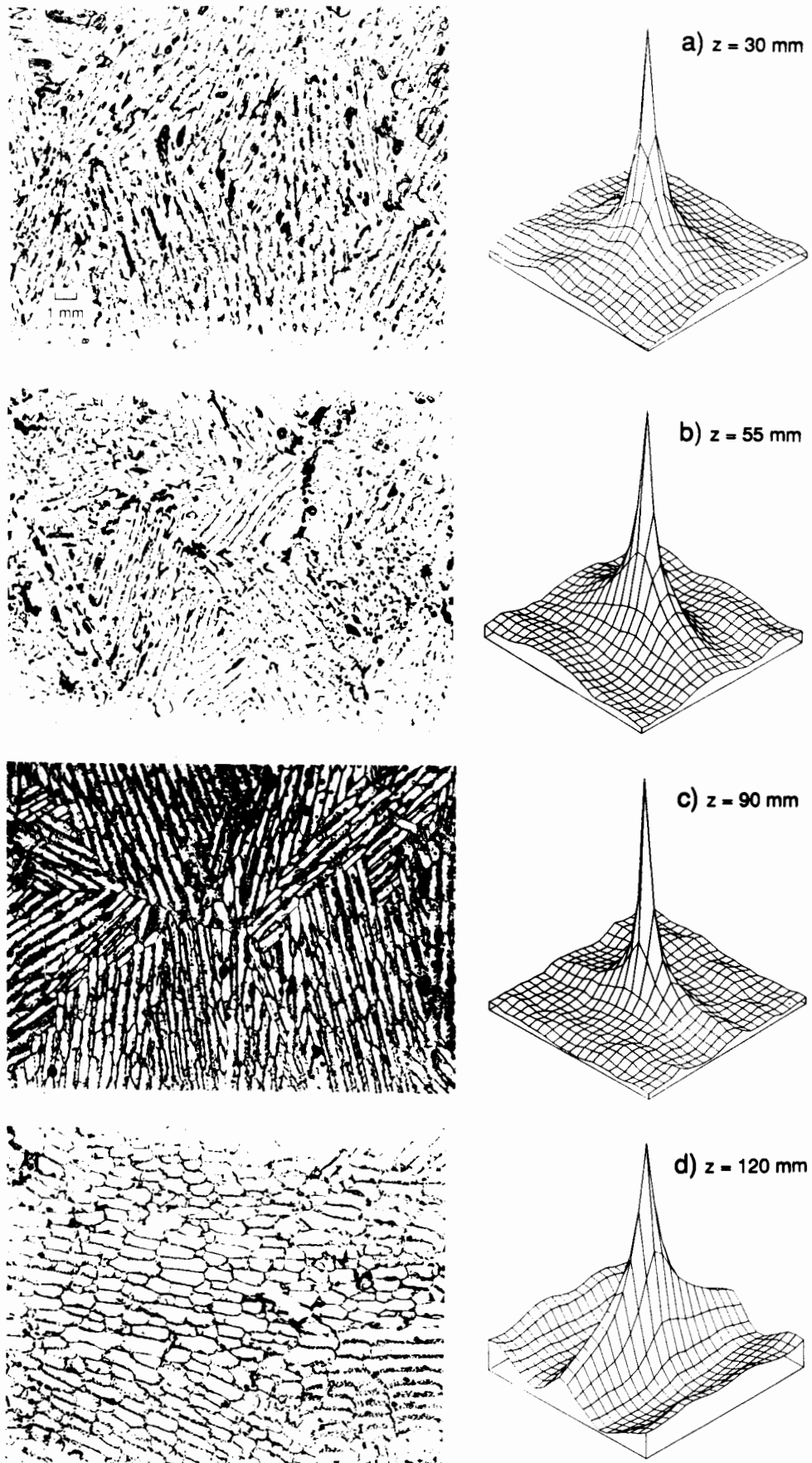


Fig. 4. A vertical profile of horizontal thin sections and correlation functions for young, columnar, saline ice. The sections were taken at depths of (a) 30 mm, (b) 55 mm, (c) 90 mm and (d) 120 mm. The horizontal scale is 1 mm.

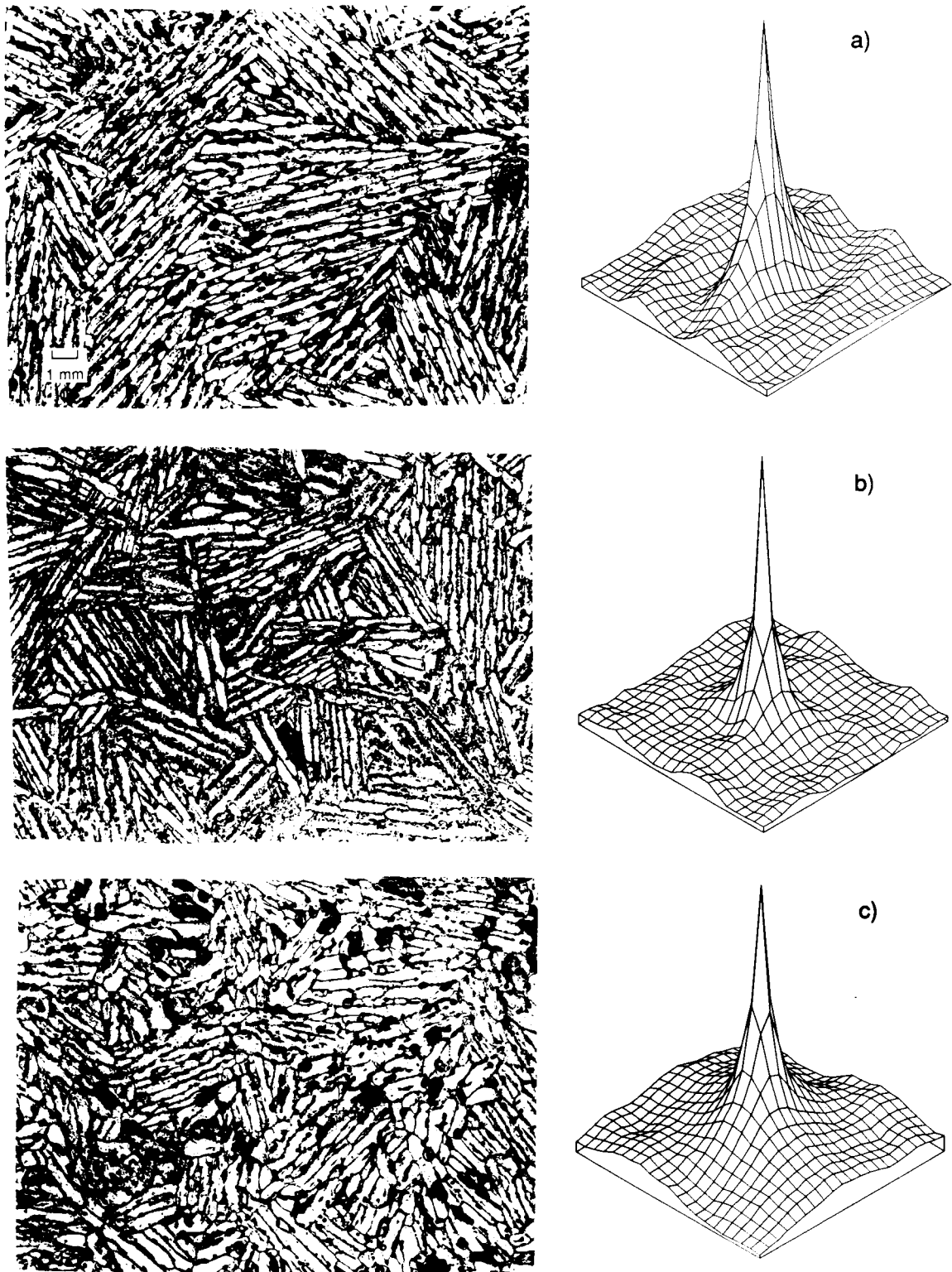


Fig. 5. The horizontal variability of ice structure and correlation function. All three sections were taken from near the bottom of a 65-mm-thick ice cover. The ice salinity was 10‰ and the sections were photographed at a temperature of -10°C . The horizontal scale is 1 mm.

coldest temperatures at the surface and the warmest at the ice-water interface, with the brine volume increasing with depth. This results in a general trend of correlation lengths increasing with depth. This trend, however, can be overridden by structural changes in the ice microstructure, such as

variations in the ice platelet diameter or a switch from columnar to granular crystals.

A critical component of this work is its incorporation into microwave models of sea ice. For example, while our results indicate that there is small-scale horizontal variability in the

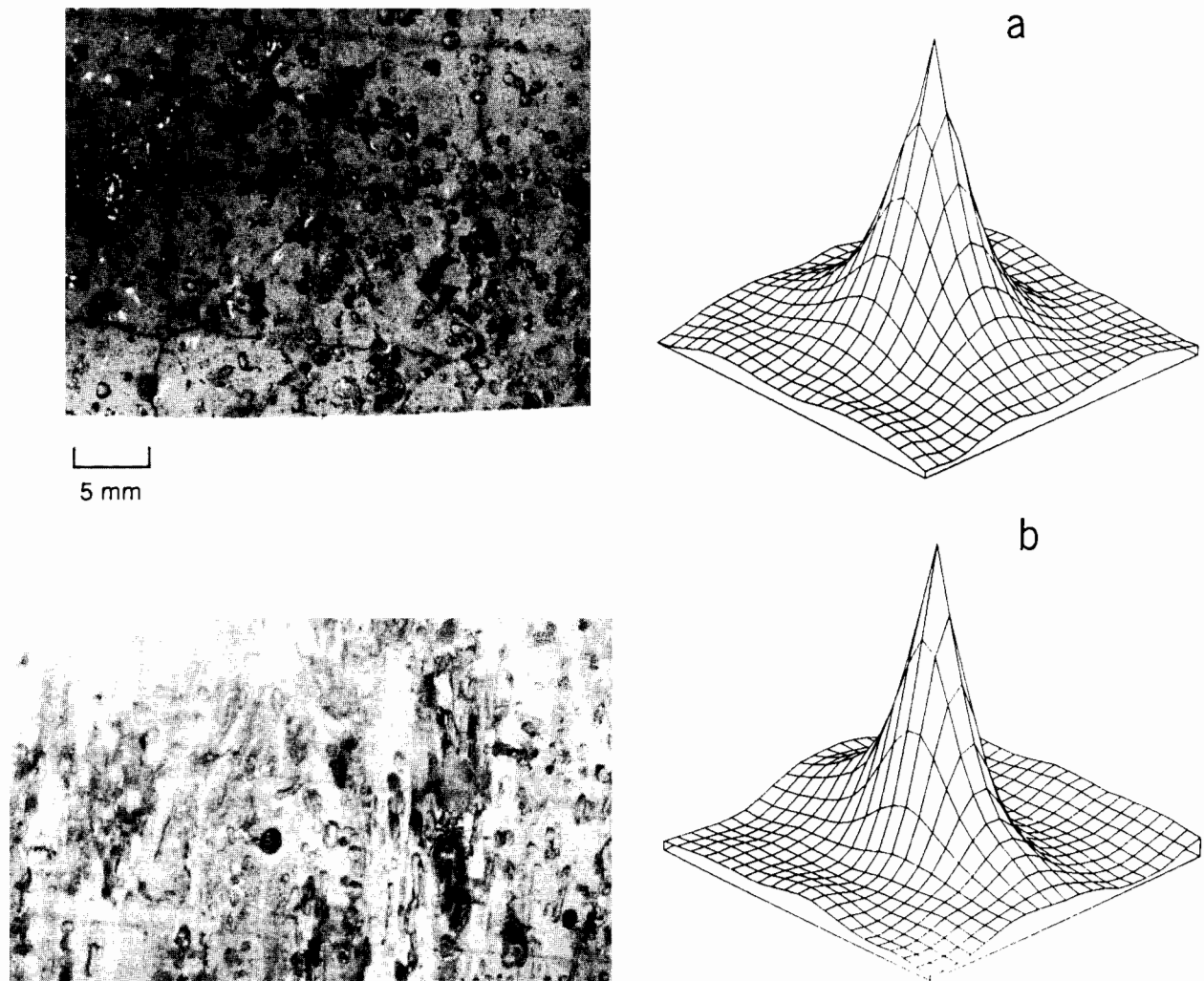


Fig. 6. Correlation functions for desalinated ice. Pictured are thin section photographs and correlation functions for (a) a horizontal thin section in the upper few millimeters and (b) a vertical thin section of the upper layer of a desalinated ice cover.

correlation function, modeling sensitivity studies are needed to ascertain if these differences significantly affect the microwave signatures of the medium. Data from the CRRELEX pond experiments [Grenfell and Comiso, 1986; Arcone *et al.*, 1986] are particularly well suited for model development and evaluation, since they were part of a large multidisciplinary effort, which also included passive and active microwave measurements as well as the detailed description of the ice structure. Additional future work needs to address (1) correlation functions in the vertical plane, (2) the determination of other statistical measures, such as inclusion size distributions and (3) examination of other ice types and conditions with a goal of generalizing the results.

Using standard thin sectioning procedures and a computer-based image processing system it is straightforward, though somewhat time-consuming, to compute the mean and variance of the permittivity and two-dimensional correlation functions in the horizontal plane. As was discussed earlier, because of the vertical orientation of the ice platelets in saline columnar ice, a single vertical section is not as well suited crystallographically as a horizontal section for examining brine inclusion characteristics. However, information on vertical as well as horizontal correlation lengths is needed

for random media modeling. A true three-dimensional analysis consisting of a series of vertical sections from the same piece of ice could provide sufficient data in the vertical direction. Thus an alternative means of determining the spatial distribution of ice and brine that does not require thin sectioning of the ice would be desirable.

An intriguing possibility is the use of a computerized axial tomography (CAT) X ray scanner. Such scanners are used routinely in medicine and their application to studying sea ice structure and ice sheet core structure has been reported by Kawamura [1988, 1990]. In this method an ice core can be scanned either horizontally or vertically at intervals equal to the X ray beam thickness (typically millimeters). These two-dimensional slices are stored in digital form so they can be combined to give a full three-dimensional image, from which correlation functions and other statistical parameters can be computed. Kawamura [1988] has shown that ice, brine and air can easily be distinguished, since they have different X ray absorption coefficients. Potentially this method has three major advantages: (1) it is nondestructive, (2) a full three-dimensional analysis can be performed and (3) it is possible to distinguish between three constituent components, ice, brine and air, more accurately than by using

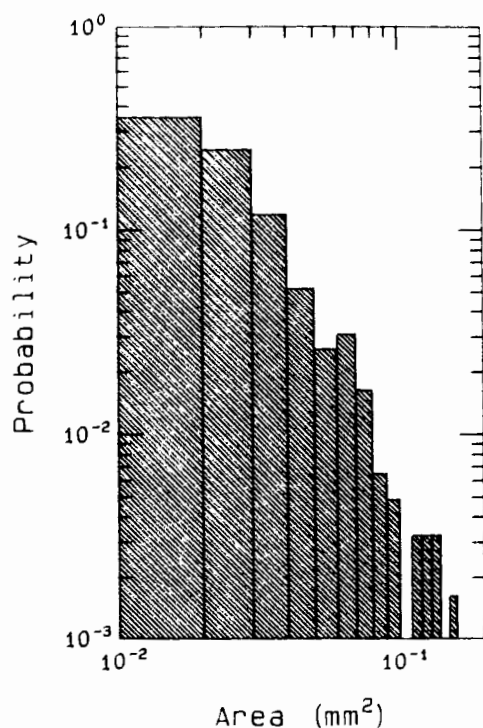


Fig. 7. Brine inclusion size distribution for sample case presented in Figure 1.

visual techniques. At present the method is limited by its cost, which precludes routine analysis of many samples, and by its limited spatial resolution of approximately 1 mm. If scanners with improved spatial resolution become available, selected studies of three-dimensional correlation functions could be performed. Another common medical diagnostic tool, magnetic resonance imagery (MRI) offers another possible, noninvasive means of determining the ice microstructure.

While the focus of this paper has been on correlation functions and the application to strong fluctuation theory microwave modeling, there are many other possible statistical descriptions and many other applications. For example, Winebrenner *et al.* [1989] discussed the importance of air bubble size distributions in dense medium radiative transfer microwave models. At optical wavelengths, the significance of the air bubble size distribution for fresh ice [Mullen and Warren, 1988] and the brine pocket distribution for sea ice [Perovich and Grenfell, 1981; Grenfell, 1983] is well known. What is not well known is the nature of these distributions.

An advantage of our methodology is that it is fairly simple to determine additional statistical measures once the image is digitized. As an example of this, Figure 7 shows the brine inclusion size distribution for the thin section presented in Figure 1. The size distribution was automatically determined by software using the ice-brine partitioned image in Figure 1c. This 270-mm² section had 615 inclusions with a total area 17 mm² and a mean area of 0.028 mm². If we assume that the inclusions were elliptical with an aspect ratio of 1.25, as the correlation lengths indicated, then the mean values of the major and minor axes were 0.10 and 0.08 mm. Though somewhat smaller, these values are roughly comparable to the correlation lengths (0.15, 0.12) determined for this image. The size distribution shows a sharp dropoff of probability (P)

as the area (A) of the brine inclusion increases and can be approximated by a power law with $P = 1.9 \times 10^{-5} A^{-2.5}$ ($R^2 = 0.96$).

Statistical descriptions for other ice types need to be investigated. Two ice types of particular interest are the drained low-density layer of multiyear ice and young frazil ice. The low-density surface layer is believed to have a major impact on radar backscatter (R. Onstott, personal communication, 1991). Frazil ice coverage is extensive in the Southern Ocean, comprising, for example over 50% of the sea ice cover in the Weddell Sea, Antarctica [Gow *et al.*, 1987]. In the Arctic, frazil is somewhat less common, but still accounts for approximately 20% of the ice cover [Tucker *et al.*, 1987].

So little is known regarding statistical descriptions of ice microstructure that additional data are useful for survey purposes. However, because of the large areal coverage of microwave remote sensing devices, a detailed description of all the ice observed is impossible. Therefore it is important that the available statistical descriptions be used to achieve a better understanding of the processes involved in determining the ice microstructure, enabling the results to be placed in a broader context. Ideally, this broader context would entail formulating a theoretical model describing ice microstructure. For example, Cox and Weeks [1989] developed a model which predicts temperature, salinity and brine volume profiles for growing first-year ice. Coupling the Cox and Weeks model with the appropriate ice microstructure statistics, it might be possible to extend their model to predict not only the volume of the brine, but the distribution of the brine as well. With additional work the effects of a melt season might also be included to provide an estimate of the air volume and the size distribution of air bubbles.

Acknowledgments. The authors would like to express their extreme gratitude to J. Kong for his many helpful suggestions and encouragement in this study. We would also like to acknowledge the efforts of H. Greeley and A. Hirai in the development of the image processing software. This work was funded by the Office of Naval Research under contract N000148WRM24001.

REFERENCES

- Arcone, S. A., A. J. Gow, and S. McGrew, Structure and dielectric properties at 4.8 and 9.5 GHz of saline ice, *J. Geophys. Res.*, 91, 14,281–14,303, 1986.
- Cox, G. F. N., and W. F. Weeks, Numerical simulations of the profile properties of undeformed first-year sea ice during the growth season, *J. Geophys. Res.*, 93, 12,449–12,461, 1988.
- Frankenstein, G. E., and R. Gardner, Equations for determining the brine volume of sea ice from -0.5°C to -22.9°C , *J. Glaciol.*, 6, 943–944, 1967.
- Gow, A. J., S. F. Ackley, K. Buck, K. Golden, Physical and structural characteristics of Weddell Sea pack ice, *Rep. 87-14*, U.S. Army Cold Reg. Res. and Eng. Lab., Hanover, N. H., 1987.
- Grenfell, T. C., A theoretical model of the optical properties of sea ice in the visible and near infrared, *J. Geophys. Res.*, 88, 9723–9735, 1983.
- Grenfell, T. C., and J. C. Comiso, Multifrequency passive microwave observations of first-year sea ice growth in a tank, *IEEE Trans. Geosci. Remote Sens.*, GE-24, 826–831, 1986.
- Kawamura, T., Observations of the internal structure of sea ice by X ray computed tomography, *J. Geophys. Res.*, 93, 2343–2350, 1988.
- Kawamura, T., Nondestructive, three-dimensional density measurements of ice core samples by X ray computed tomography, *J. Geophys. Res.*, 95, 12,407–12,412, 1990.
- Lin, F. C., J. A. Kong, R. T. Shin, A. J. Gow, and S. A. Arcone,

- Correlation function study for sea ice, *J. Geophys. Res.*, *93*, 14,055–14,063, 1988.
- Mullen, P. C., and S. G. Warren. Theory of the optical properties of lake ice, *J. Geophys. Res.*, *93*, 8403–8414, 1988.
- Papoulis, A., *Probability, Random Variables and Stochastic Processes*, McGraw-Hill, New York, 1965.
- Perovich, D. K., and T. C. Grenfell. Laboratory studies of the optical properties of young sea ice, *J. Glaciol.*, *27*, 331–346, 1981.
- Perovich, D. K., and A. Hirai. Microcomputer-based image-processing systems, *J. Glaciol.*, *34*, 249–252, 1988.
- Stogryn, A., Correlation functions for random granular media in strong fluctuation theory, *IEEE Trans. Geosci. Remote Sens.*, *GE-22*, 150–154, 1984.
- Tsang, L., and J. A. Kong. Scattering of electromagnetic waves from random media with strong permittivity fluctuations, *Radio Sci.*, *16*, 303–320, 1981.
- Tsang, L., J. A. Kong, and R. T. Shin, *Theory of Microwave Remote Sensing*, Wiley Interscience, New York, 1985.
- Tucker, W. B., III, J. A. Richter-Menge, and A. J. Gow. On small-scale horizontal variations of salinity in first-year sea ice, *J. Geophys. Res.*, *89*, 6505–6514, 1984.
- Tucker, W. B., III, A. J. Gow, and W. F. Weeks. Physical properties of summer sea ice in the Fram Strait, *J. Geophys. Res.*, *92*, 6787–6803, 1987.
- Tucker, W. B., III, T. C. Grenfell, R. G. Onstott, D. K. Perovich, A. J. Gow, R. A. Shuchman, and L. L. Sutherland. Microwave and physical properties of sea ice in the winter marginal ice zone, *J. Geophys. Res.*, *96*(C3), 4573–4587, 1991.
- Untersteiner, N., Natural desalination and equilibrium salinity profile of old sea ice, *J. Geophys. Res.*, *73*, 1251–1257, 1968.
- Vallese, F., and J. A. Kong. Correlation function studies for snow and ice, *J. Appl. Phys.*, *52*, 4921–4925, 1981.
- Vant, M. R., R. O. Ramseier, and V. Makios. The complex dielectric constant of sea ice at frequencies in the range 0.1–40 GHz, *J. Appl. Phys.*, *49*, 4712–4717, 1978.
- Winebrenner, D. P., L. Tsang, B. Wen, and R. West. Sea ice characterization measurements needed for testing of microwave remote sensing models, *IEEE J. Oceanic Eng.*, *14*, 149–158, 1989.
- A. J. Gow and D. K. Perovich, U.S. Army Cold Regions Research and Engineering Laboratory, 72 Lyme Road, Hanover, NH 03755.

(Received February 6, 1991;
revised June 7, 1991;
accepted June 11, 1991.)